SLAC-PUB-10137

Analysis of x-ray diffraction as a probe of interdiffusion in Si/SiGe heterostructures

D.B. Aubertine, N. Ozguven, and P.C. McIntyre
Department of Materials Science and Engineering
Stanford University, Stanford, CA

S. Brennan
Stanford Synchrotron Radiation Laboratory
Stanford Linear Accelerator Center, Stanford, CA

We investigate numerical simulations that utilize a non-linear interdiffusion solver and dynamical x-ray diffraction calculations to predict the local composition evolution in low Ge concentration Si/SiGe superlattices and their diffraction patterns during annealing. Superlattice satellite peak decay rates are compared with experimentally measured values and simulated diffraction patterns are matched directly to data with good success. The simulations are used to test the sensitivity of x-ray diffraction to various uncertainties commonly encountered when measuring interdiffusion at Si/SiGe interfaces. It is found that the most serious errors result from variations in the Ge content across the surface of the wafer. For example, the resolution limit of most experimental techniques used to measure Ge concentration in a SiGe film is − 1 at.%, for a film with 11% mean Ge concentration annealed for 5 hours at 870…C, this level of error will cause the observed interdiffusivity values to deviate by —25% or +50%. The simulations are further used to show that for Si/SiGe interdiffusion, superlattice diffraction produces valid measurements when applied to 004 superlattice satellite peaks and square wave composition modulations even though it is only exactly applicable to satellite peaks about 000 reflection and to sinusoidal composition modulations. Finally, we show that proper interpretation of x-ray scattering data to extract Si/SiGe interdiffusivity values must account for the strong dependence of the interdiffusivity on Ge concentration.

Work supported in part by Department of Energy Contract DE-AC03-76SF00515

1. Introduction

Silicon germanium alloys have become important materials for semiconductor device engineering. They provide a means of tailoring the properties of the semiconductor, such as band-gap, carrier mobility, and dopant solubility at specific locations within a device. Further, these benefits are realized at a relatively low cost owing to the high degree of compatibility between SiGe and Si processing technologies.

As SiGe technology matures it is becoming increasingly important to be able to determine the allowable thermal budgets for newly developed device structures. In addition to the frequently discussed high temperature stability problems of dopant diffusion and strain relaxation, Si/SiGe interfaces are also vulnerable to Ge out-diffusion. For example, interdiffusion at the interface between a relaxed SiGe buffer layer and a Si channel strained in tension degrades the mobility in the channel both by creating a gradual interface[1] and by depositing Ge atoms inside the channel causing alloy scattering.[2,3] As an illustration of the potential severity of this problem, several groups have found that a 10 nm strained Si channel grown on a $Si_{0.7-0.8}Ge_{0.3-0.2}$ relaxed buffer layer is largely washed out after a 30 second anneal at 1000 C.[3-5] X-ray diffraction is a powerful tool for studying interdiffusion in Si/SiGe heterostructures and in this paper we investigate several key issues related to its use and interpretation.

Interdiffusion at Si/SiGe interfaces exhibits a complicated concentration dependence and can not be treated with linear diffusion calculations.[6] Both the exponential prefactor and

activation enthalpy for interdiffusion are concentration dependent.[7-10] The interdiffusivity is modified by film strain, which is a function of both Ge concentration and the density of misfit dislocations at the film substrate interface.[8,9,11] Finally, the degree to which the interdiffusion is controlled by an interstitial or vacancy mechanism changes as a function of the Ge concentration.[10] Before interdiffusion at Si/SiGe interfaces can be successfully modeled, each of these couplings between Ge concentration and interdiffusivity must be isolated and thoroughly studied, a process that has only just begun.

There are a number of techniques available for measuring interdiffusion at Si/SiGe interfaces. The most common approach is to perform direct measurements of the Ge profile across a Si/SiGe interface as a function of annealing time. This type of work can be performed with Rutherford backscattering spectrometry (RBS), cross sectional transmission electron microscopy (XTEM), thin sectioning by mechanical means or via ion etching, and most frequently with secondary ion mass spectrometry (SIMS). While valuable experiments are often performed in this manner, the sensitivity to interdiffusion is limited by the composition and depth resolution of the technique employed. By comparison, x-ray diffraction (XRD) measurements of Si/SiGe superlattices are sensitive to much lower values of interdiffusivity; values as low as 10^{20} cm^2/s have been measured in this manner.[12] Unlike the techniques discussed above, for which the spatial resolution of the depth profiles are limited by the instrument, with x-ray diffraction, it is limited by the quality and uniformity of the interfaces within the superlattice. Given the advanced state of Si and SiGe epitaxial deposition technologies, sub-nanometer diffusion lengths

are readily accessible by the x-ray scattering technique. In addition, it provides a simultaneous probe of both interdiffusion and strain relaxation in epitaxial heterostructures.

X-ray diffraction measurements of interdiffusion in Si/SiGe require the use of a superlattice structure. For an 001-oriented Si/SiGe superlattice, interdiffusion measurements are based on recording the decay of superlattice satellite peaks about the 000 (direct beam) or 004 Bragg reflection as a function of annealing time. In a system with concentration independent interdiffusivity and zero lattice mismatch, assuming sinusoidal composition modulation, the interdiffusivity is proportional to the natural logarithm of the first order satellite decay rate according to:

$$\frac{d}{dt}\ln\left(\frac{I(t)}{I(0)}\right)=\frac{-8\pi^2}{\lambda^2}\tilde{D}_\lambda \qquad \text{Eq. 1}$$

where *I(t)* is the superlattice satellite intensity as a function of annealing time, *t*, and l is the spatial period of the superlattice.[12]

In this paper we present three main points relating to the measurement of interdiffusion via XRD. First, we describe simulation methods capable of performing a full virtual interdiffusion experiment. Given an experimentally determined, as-grown composition profile, a numerical non-linear diffusion calculation is performed to predict the evolution of the profile as a function of simulated annealing time. A numerical, dynamical XRD simulator is then applied to the evolving composition/strain profile to extract simulated

diffraction patterns. Second, we compare simulated results to experimental data collected from Si/SiGe epitaxial multilayers in order to evaluate the effectiveness of the simulations. Finally, using insights obtained from the simulations, we investigate several important issues relating to the effectiveness of XRD as a measurement technique for interdiffusion at Si/SiGe interfaces.

2. Experiment and simulation

2.1. Empirical work

For comparison with the simulation results presented in this paper, we performed measurements on a series of low concentration Si/SiGe superlattices grown directly onto 001 Si substrates. The example shown in Fig. 1 is characteristic of the samples examined. In every case the thickness of the overall film on the Si substrate is supercritical with respect to the formation of misfit dislocations, however the individual SiGe alloy layers within the multilayer are subcritical. Our critical thickness calculations and characterization of strain relaxation in these samples as a function of annealing time are discussed in previously published work.[6]

The Si/SiGe superlattice samples examined here were grown by either reduced pressure chemical vapor deposition (RPCVD) or ultra high vacuum chemical vapor deposition (UHVCVD). The RPCVD samples were grown in an ASM Epsilon II Epitaxial Reactor at the Stanford Nanofabrication Facility. The growth was performed at 625 C, in a 15

Torr, hydrogen ambient. Dichlorosilane and germane were used as growth gases. The UHVCVD samples were grown at 550 C with silane and germane growth gases. Further details of the UHVCVD growth process are published elsewhere.[13] In every case, both the underlying Si material and the Si/SiGe superlattice were undoped.

Structural characterization was performed primarily by XRD. Triple axis, non-symmetric diffraction studies were used to measure the average in-plane and out-of-plane lattice parameters in order to determine the average composition and strain state of the as-grown films. For this we utilized the experimental geometry presented by Van der Sluis et al[14] and the elasticity analysis of Bugiel et al.[15] We also confirmed the average film composition via Rutherford backscattering spectrometry (RBS). Both techniques have a composition resolution of about one atomic percent and in every case the results agreed to within experimental error. The spatial periodicity and overall film thickness of each superlattice were determined from the superlattice satellite and thickness oscillation spacing about the 004 Bragg reflections as discussed by Bowen et al.[16] Cross-sectional transmission electron microscopy (XTEM) was used to assess the thickness ratio of the Si and SiGe layers within each superlattice bilayer as well as the lateral and layer-to-layer variation in bilayer thickness.

After growth and characterization, wafers were cleaved into pieces of approximately one square centimeter and annealed in a quartz tube furnace using an ultra high purity nitrogen ambient. The temperature range for annealing experiments, 795 C to 895 C, was selected because it provided interdiffusion rates that were not so slow as to yield no

change in XRD measurements in a reasonable amount of time, and not so fast as to be difficult to study accurately using tube furnace anneals.

Interdiffusion measurements were performed via high-angle, symmetric, XRD studies both on the 4-circle Philips X Pert system in the Geballe Laboratory for Advanced Materials and on the 2-circle diffractometer at beam line 2-1 of the Stanford Synchrotron Radiation Laboratory. Both systems were configured in a triple axis geometry. The X Pert system utilized Cu K_{a1} radiation with a four-bounce (220) Ge monochromator and a two-bounce, channel cut, (220) Ge analyzer crystal. Beam line 2-1 employed 7000 eV radiation with a Si (111) analyzer crystal.

2.2 Simulation work

The simulations investigated in this work involved calculations of both diffusion and XRD. After accepting input parameters to define a sample structure, annealing conditions, and details of the diffraction experiment, the interdiffusion code first computed the evolution of the composition profile as a function of annealing time, then sent a composition-position-time matrix to the XRD simulator which produced a diffracted intensity-scattering vector-time matrix. Several sample-specific input parameters were required to define the starting conditions for each simulation. These included the number of bilayers, the bilayer thickness, the Ge composition in the SiGe layers, the Si to SiGe layer thickness ratio, the as-grown interfacial width and profile shape, the degree of strain relaxation in the as-grown sample, the annealing temperature

as a function of time, the degree of strain relaxation as a function of annealing time, the x-ray wavelength, and the x-ray beam divergence.

As discussed previously,[6] the interdiffusivity was calculated according to —

$$\tilde{D} = \tilde{D}_0 \exp\left(\frac{-\Delta H_a}{k_b T}\right) \qquad \text{Eq. 2a}$$

$$\tilde{D}_0 = A_{D0} \exp\left(-B_{D0} X_{Ge}\right)\left(1 - \frac{\alpha X_{Ge} X_{Si}}{k_b T}\right) \qquad \text{Eq. 2b}$$

$$\Delta H_a = \Delta H_a^{self} + Q'\left(-0.042 X_{Ge} + \varepsilon_{dislocation}\right) \qquad \text{Eq. 2c}$$

where a is the enthalpy of mixing coefficient for the alloy, X_i is the atomic fraction of element i, A_{D0} and B_{D0} are empirical fitting parameters that define the curve fit in Fig. 2, ΔH_a^{self} is the concentration dependent activation enthalpy for SiGe self-diffusion shown in Fig. 3, Q is a proportionality constant relating activation enthalpy to biaxial film strain, and $\varepsilon_{dislocation}$ is the strain relieved by misfit dislocations at the film/substrate interface. A complete treatment of the exponential prefactor for interdiffusivity includes both Kirkendal and Darken terms as shown in Eq. 3

$$\tilde{D}_0 = \left(D_{Ge} X_{Si} + D_{Si} X_{Ge}\right)\left(1 - \frac{\alpha X_{Ge} X_{Si}}{k_b T}\right) \qquad \text{Eq. 3}$$

where D_i is the tracer diffusivity of element i in a SiGe alloy of concentration X_{Ge} We arrive at the form for the exponential prefactor given in Eq. 2(b) by assuming that the tracer diffusivities of Si and Ge are essentially equal in SiGe and decrease exponentially as a function of Ge concentration. These assumptions were discussed in our previous work[6] and are further supported by recent experimental measurements reported by

Strohm et al.[10] showing that the activation enthalpy and exponential prefactor for self-diffusion are similar for Si and Ge in SiGe alloys. The exponential prefactor and activation enthalpy values incorporated into our simulation model were taken from the work of Zangenberg et al.[8] who used SIMS to measure the intermixing of isotopically distinct, but chemically identical SiGe layers in strain relaxed films. We arrived at Eq. 2(c) by following the theoretical work of Aziz[11] who found that the activation enthalpy for Si/SiGe interdiffusion should be linearly proportional to biaxial film strain. Unfortunately, the proportionality constant has yet to be clearly established. Empirically derived values reported in the literature range between 19 and 160 eV/unit biaxial compressive strain.[8,17] Recent theoretical work by Ramanarayanan et al[18] yielded a value of 17 to 20 eV/unit strain. We used a value of 25 eV/unit strain because it was most consistent with reported values for the activation enthalpy and exponential prefactor for Si/SiGe interdiffusion as discussed in our previous work.[6]

The diffusion calculation was performed for a single superlattice bilayer positioned symmetrically about the center of a SiGe layer. This allowed periodic boundary conditions to be applied. Once the evolution of the composition profile in the bilayer was calculated, an entire superlattice could be assembled by attaching the appropriate number of bilayers end to end. Because this approach neglected diffusion from the superlattice into the substrate, we took the additional step of running a second diffusion calculation to simulate the evolution of the lowest bilayer. In this case we began with the same initial concentration profile but applied new boundary conditions. The left side was allowed to diffuse into an infinitely thick region of pure Si, which represented the substrate, and the

right side was matched to the concentration at the edge of the neighboring bilayer. Although the right-side boundary condition was somewhat artificial, the simulation was always stopped before the peak concentration in this lowermost bilayer droped below that of its neighbors.

Both the interfacial abruptness and the measured interlayer thickness variations were combined into a single characteristic interfacial width for the purpose of defining the as-grown structure. Typically a sinusoidal shape was used for the interfacial region but several other shapes including a straight line, a sinusoid, and an error-function were also tried. Simulated as-grown and interdiffused profiles are shown in Fig. 4.

Specular reflectivity about the 004 Bragg reflection was simulated using the recursive formalism for dynamical diffraction simulation described by Bartels, et al.[19] Results using this simulation package have been presented previously.[20] Because this formalism requires matching the x-ray amplitude and phase at each interface, the interdiffused superlattice structure was broken into a series of finite slabs of uniform concentration (typically about 100 slabs per bilayer) and input into the diffraction simulation code as a discrete structure. The measured values for strain relaxation as a function of annealing time were incorporated by varying a coherency parameter that ranged from one for a fully coherent film to zero for a fully relaxed film. An example of output from the diffraction simulator is given in Fig. 5.

The simulation results were compared with experimental data in two different ways. First, the natural logarithm of the minus one superlattice satellite peak decay rate was compared with experimental values. Simulated satellite peak intensities were normalized by the film peak intensity in exactly the same manner as the experimental data. If Eq. 1 holds, an assumption addressed later in this paper, the slope of these curves should be linearly proportional to the interdiffusivity at time *t*. A characteristic example is illustrated in Fig. 6. Second, the simulated diffraction patterns were formatted according to procedures defined by Bowen et al.[16] and overlaid directly onto experimentally derived diffraction patterns. First, the simulated pattern was normalized to the intensity of the film peak and the DC background of the experimentally derived diffraction pattern. Then, zero-centered detector noise was added to the simulated pattern. The diffraction pattern was also convolved with beam divergence. The divergence value was selected by matching the width of the simulated and measured substrate peaks. Physically, this accounted for both the finite divergence of the beam conditioner and the effects of sample curvature.

To minimize experimental non-idealities, certain precautions were taken when recording diffraction patterns to be compared with a simulation. A triple axis diffraction geometry was used in a symmetric configuration to eliminate the effects of diffuse scatter, to reduce background noise, and to minimize the loss of fine detail that occurs in double axis rocking curves.[16] To remove the effects of tilts in the superlattice structures, a full 004 high resolution reciprocal space map was taken and the diffraction pattern was formed by following the ridge of maximum intensity in reciprocal space. Tilts can be

introduced in the form of wafer miscut, sample mounting, and by the screw component of the interfacial misfit dislocation array.[16] Examples of overlaid experimental and simulated diffraction patterns are shown in Fig. 7.

3. Results

3.1 Simulation output

Simulated superlattice satellite decay rates were compared with experimentally measured decay rates for three separate superlattices at a number of annealing temperatures between 795 C and 870 C. The superlattices examined had the following structures — [Si 5 nm $Si_{0.87}Ge_{0.13}$ 5.6 nm]$_{10}$, [Si 3.3 nm $Si_{0.85}Ge_{0.15}$ 10.2 nm]$_{12}$, and [Si 2.2 nm $Si_{0.85}Ge_{0.15}$ 6.1 nm]$_{20}$. As an example, the results for the 20-bilayer structure are shown in Fig. 6. Data sets from all three samples agreed well with the simulations.

Experimentally derived and simulated diffraction patterns were compared directly for a number of as-grown and annealed cases. Three examples are illustrated in Fig. 6. It is significant that the structural parameters used as inputs to the diffraction simulator were determined independently from the simulations and were not corrected in order to optimize the fit. We generally found good agreement in relative satellite peak intensities and some discrepancy in satellite peak positions, especially for higher order satellites. Intensities in the region between the satellite peaks matched the data very well in some

cases and poorly in others. The examples presented in Fig. 7(a) and 7(c) correspond to best and worst case scenarios in this regard.

3.2 Sensitivity to experimental non-idealities

To assess the sensitivity of XRD as a probe of interdiffusion at Si/SiGe interfaces with respect to various experimental non-idealities, the simulation presented in Figs. 4 — 6 was rerun with various parameters perturbed. To quantify the sensitivity to a perturbed variable, we used as a metric the accumulated error in the interdiffusivity value, 8.6 · 10^{-19} cm^2/s, extracted from the superlattice satellite decay rate after a five hour anneal at 870 C.

First, we examined the importance of the interfacial width and shape used as initial conditions for the interdiffusion calculations. As previously discussed, every interface in the as-grown concentration profile was assigned a finite thickness that was extracted from cross sectional TEM micrographs of the structure; the thickness was typically a few nanometers. We found that the extracted interdiffusivity value was largely independent of the interfacial profile shape and only weakly sensitive to the interfacial thickness — setting the thickness to zero or quadrupling it produced errors of less than 5%.

One of the simulation inputs was the degree of strain relaxation as a function of annealing time. The initial, average, coherency biaxial strain was —0.0047. After 5 hours at 870 C, 4% of this coherency strain was found to have relaxed. To test the importance of

determining this value accurately, we ran the simulation with zero strain relaxation and 20% strain relaxation. The former case yielded a 2% increase in interdiffusivity and the latter a 10% decrease.

To test the importance of annealing temperature calibration, we ran the simulation for temperatures of 865 C and 875 C. These adjustments yielded changes in the interdiffusivity relative to the results at 870 C of -4% and +13% respectively.

There is always a certain variation in Si/SiGe heterostructure thickness across a wafer surface. Using XRD, we recorded a full wafer map on a film similar to that shown in Fig. 1 and found that, excluding the near-edge region of the wafer, the bilayer thickness varied by ~ − 1 nm. By adjusting the simulation parameters accordingly we determined that ignoring this degree of thickness variation could cause an error of about 15% in the measured interdiffusivity.

Finally, we checked the sensitivity of the extracted interdiffusivity to errors in the Ge concentration. Because most measurement techniques, including the XRD that was employed in this study, can only determine a SiGe film s Ge concentration to − 1 %, we ran simulations with this level of error. We found that under-estimating and over-estimating the average film composition by 1% caused -25% and +50% errors in the interdiffusivity respectively.

3.3 Effects of a concentration dependent interdiffusivity

Figure 8 shows the difference in simulated superlattice satellite decay results for a constant and a concentration-dependent interdiffusivity. Both simulations were run for the superlattice structure illustrated in Fig. 1. For the concentration independent case we fixed the exponential prefactor and activation enthalpy at values appropriate for Si self-diffusion. Three trends are plotted for each case. The first trend shows the interdiffusivity values used by the interdiffusion simulation at each time step (diffusion model output). The second trend indicates the interdiffusivity extracted by applying a finite Fourier transform to the concentration profile at each time step and tracking the decay of the resulting first order Fourier peak (FFT result). The third trend gives the interdiffusivity extracted from the simulated superlattice satellite peak decay rates (XRD simulation). The results in fig. 8(b) are for a concentration-dependent interdiffusivity. In this case a range of interdiffusivity values were used by the model corresponding to the range of Ge concentrations present in the film at each time step. To illustrate this, three different model result trends are shown. The first shows the interdiffusivity value appropriate for the average Ge concentration present at each time step, the second and third show interdiffusivity values appropriate for the maximum and minimum Ge concentrations present at each time step.

Figure 9 shows the interdiffusivity values used by the interdiffusion model for the mean, maximum, and minimum Ge concentrations present in the superlattice at each simulation time step. Two cases are shown, the first corresponding to a relatively low Ge

concentration superlattice, [Si 5 nm $Si_{0.87}Ge_{0.13}$ 5.6 nm]$_{10}$, the second a higher Ge concentration superlattice, [Si 2.2 nm $Si_{0.85}Ge_{0.15}$ 6.1 nm]$_{20}$.

4. Discussion

The combined interdiffusion and XRD simulations were found to successfully reproduce the measured superlattice satellite decay results as a function of simulated annealing time. The diffraction simulator also reproduced the diffraction patterns of both as-grown and annealed samples with reasonable accuracy. Despite these successes, the simulations have been tested under a limited set of conditions and many of the assumptions utilized in the interdiffusion calculations restrict their application to films of relatively low Ge concentration. However, important observations can be drawn from the interplay between a concentration-dependent diffusion solver and a first principles dynamical diffraction simulation.

Several reservations are often expressed when Eq. 1 is applied to the analysis of interdiffusion at Si/SiGe interfaces. First, for lattice mismatched systems, the theoretical basis for the analysis is only applicable to the decay of superlattice satellites about the direct beam (000 Bragg reflection).[12] This problem was investigated experimentally for Si/SiGe interfaces by Prokes et al[21] who found that after an initial period of different time evolution, the 004 and 000 superlattice satellites decayed at the same rate. The results presented in Fig 8(a) support the idea that interdiffusivity can be extracted from the 004 superlattice satellite decay rate at all times, not just in the long-time limit. Because a

concentration independent interdiffusion simulation was used in this case, there was a single, known interdiffusivity value. That same value was then extracted from the first principles x-ray diffraction simulation. This is significant because the interdiffusivity values were never introduced as input into the x-ray simulation. Thus, we conclude that accurate interdiffuvisity data can be extracted from the decay of superlattice satellite peaks about 004 Bragg reflections.

A second issue that should be considered when applying this technique is that Eq. 1 was derived for a sinusoidal concentration modulation and it is not necessarily accurate in the presence of square wave concentration modulations like those common to high quality, abrupt Si/SiGe interfaces. Again, Fig. 8(a) shows good agreement between the theoretically correct and simulated satellite decay rates. The authors have made the same observation even when simulating fully abrupt interfaces.

It is an underlying assumption in the derivation of Eq. 1 that superlattice satellite peaks correspond directly to the Fourier coefficients of the superlattice concentration modulation.[22,23] For this reason, it seems reasonable that the decay rate of the first order peak in a finite Fourier transform (FFT) of the simulated, interdiffused concentration profiles should provide ideal input for Eq. 1. As illustrated in Fig. 8(a), this approach provided superlattice satellite decay rates that matched the theoretical values. This suggested that satellite decay rates extracted from FFT results could be used as a theoretical target for the XRD simulation results. This was helpful in the concentration-dependent case, illustrated in Fig. 8(b), where the simulation used several interdiffusivity

values at each time step depending on the local Ge concentration. The agreement between the XRD and FFT output in Fig. 8(b) suggests that XRD satellite decay results can be trusted even for concentration-dependent interdiffusion.

Because the interdiffusivity varies as a function of local Ge concentration, considerable care must be given to the interpretation of superlattice satellite decay results. As an example, Fig. 8(b) clearly illustrates that the extracted interdiffusivity cannot simply be attributed to the mean Ge concentration. Certainly superlattice satellite decay measurements yield a characteristic value for interdiffusion, but they do not contain much information about the range of interdiffusivity values.

To illustrate how sensitive the range of the interdiffusivity values can be to the sample structure, the simulation results in Fig. 9 show the interdiffusivity values for two films with slightly different composition modulation amplitudes. These values were found by applying Eq. 2 to the concentration profiles generated by the interdiffusion solver at each time step. In Fig. 9(a), the peak Ge concentration is 13% and in Fig. 9(b) it is 15%. This 2% difference clearly has a large effect. For example, in Fig. 9(a), the Ge rich regions initially have the highest interdiffusivity, but because the activation enthalpy becomes approximately constant below a Ge concentration of 12% (see Fig. 3), the exponential prefactor begins to dominate and interdiffusion is actually retarded in the Ge rich regions of this superlattice after about 10000 seconds. In Fig. 9(b) the Ge rich regions retain the higher interdiffusivity value throughout the simulation.

5. Conclusions

We have investigated combined interdiffusion and x-ray scattering simulations that compute both interdiffusion and XRD for low concentration Si/SiGe superlattices. Although our investigation of the predictive power of these simulations is at an early stage, they have already provided considerable insight into the strengths and weaknesses of XRD as a technique for measuring interdiffusion at Si/SiGe interfaces.

After examining a series of potential experimental non-idealities we find that the x-ray multilayer scattering technique is relatively insensitive to uncertainties in the strain state or the rate of strain relaxation in Si/SiGe heterostructures. We also find that annealing temperature calibration should be maintained to within − 5 C to keep the error in measured interdiffusivity below 10%. The most serious errors likely to corrupt an experimental study were found to involve an uncertainty in average film composition. However, even for a measurement-to-measurement concentration variation of − 1%, the measured interdiffusivity values should be accurate to within a factor of 2.

We find that correct interdiffusivity values can be extracted even for the decay of superlattice satellites about 004 Bragg reflections from superlattices with square wave composition profiles. This is true even though the theory supporting these measurements is only rigorously correct for 000 superlattice satellite decay and sinusoidal composition modulations.

Finally, we present some of the implications of measuring interdiffusion using XRD in a system with a strongly concentration dependent interdiffusivity. While a characteristic interdiffusivity value can be extracted, local values within the film can vary by more than an order of magnitude for the Si/SiGe heterostructures investigated in this work.

6. Acknowledgements

We wish to thank A. Vailionis of Stanford University and A. Mehta of the Stanford Synchrotron Radiation Laboratory for many fruitful discussions. We also with to thank J. Chu and P. Mooney of IBM for sample preparation and A. Marshall of Stanford University for extensive assistance with sample analysis via transmission electron microscopy. Portions of this research were carried out at the Stanford Synchrotron Radiation Laboratory, a national user facility operated by Stanford University on behalf of the U.S. Department of Energy, Office of Basic Energy Sciences. D.B. Aubertine gratefully acknowledges the financial support of a National Science Foundation Graduate Fellowship. This work was funded by the Department of Energy Basic Energy Sciences grant DE-FG03-99ER45788.

References

[1] M. Miyao, K. Nakagawa, N. Sugii, and S. Yamaguchi, Microelectronic Engineering **47,** 221-3 (1999).

[2] C. W. Leitz, M. T. Currie, M. L. Lee, Z. Y. Cheng, D. A. Antoniadis, and E. A. Fitzgerald, Journal of Applied Physics **92,** 3745-51 (2002).

[3] M. T. Currie, C. W. Leitz, T. A. Langdo, G. Taraschi, E. A. Fitzgerald, and D. A. Antoniadis, Journal of Vacuum Science & Technology B (Microelectronics and Nanometer Structures) **19,** 2268-79 (2001).

[4] S. J. Koester, K. Rim, J. O. Chu, P. M. Mooney, J. A. Ott, and M. A. Hargrove, Applied Physics Letters **79,** 2148-50 (2001).

[5] H. Klauk, T. N. Jackson, S. F. Nelson, and J. O. Chu, Applied Physics Letters **68,** 1975-7 (1996).

[6] D. B. Aubertine, M. A. Mander, N. Ozguven, A. F. Marshall, P. C. McIntyre, J. O. Chu, and P. M. Mooney, Journal of Applied Physics **92,** 5027-5035 (2002).

[7] G. L. Mcvay and A. R. Ducharme, Physical Review B **9,** 627-631 (1974).

[8] N. R. Zangenberg, J. L. Hansen, J. Fage-Pedersen, and A. N. Larsen, Physical Review Letters **8712,** 5901-+ (2001).

[9] N. E. B. Cowern, W. J. Kersten, R. C. M. De Kruif, J. G. M. Van Berkum, W. B. De Boer, D. J. Gravesteijn, and C. W. T. Bulle-Liewma, in *Interdiffusion mechanisms in coherently strained SiGe multilayers*, Pennington, NJ, USA, 1996 (Electrochem. Soc), p. p 195-209.

[10] A. Strohm, T. Voss, W. Frank, P. Laitinen, and J. Raisanen, Zeitschrift fur Metallkunde **93,** 737-44 (2002).

[11] M. J. Aziz, Applied Physics Letters **70,** 2810-2812 (1997).

[12] A.L. Greer and F. Spaepen in *Synthetic Modulated Structures*; edited by A. L. Greer and F. Spaepen (Academic Press, Orlando, 1985).

[13] P. M. C. Mooney, J. O., Annual Review of Materials Science **30,** 335-362 (2000).

[14] P. van der Sluis, Journal of Physics D (Applied Physics) **26,** A188-91 (1993).

[15] E. Bugiel and P. Zaumseil, Applied Physics Letters **62,** 2051-3 (1993).

[16] D. K. Bowen and B. K. Tanner, *High resolution X-ray diffractometry and topography* (Taylor & Francis, London ; Bristol, PA, 1998).

[17] N. E. B. Cowern, P. C. Zalm, P. Vandersluis, D. J. Gravesteijn, and W. B. Deboer, Physical Review Letters **72,** 2585-2588 (1994).

[18] P. Ramanarayanan and K. Cho, unpublished work (2002).

[19] W. J. Bartels, J. Hornstra, and D. J. W. Lobeek, Acta Crystallographica, Section A (Foundations of Crystallography) **A42,** 539-45 (1986).

[20] A. Lessmann, S. Brennan, A. Munkholm, M. Schuster, H. Riechert, and G. Materlik, Physical Review B (Condensed Matter) **59,** 10801-10 (1999).

[21] S. M. Prokes, M. Fatemi, and K. L. Wang, Journal of Vacuum Science & Technology B (Microelectronics Processing and Phenomena) **8,** 254-7 (1990).

[22] E. M. Philofsky and J. E. Hilliard, Journal of Applied Physics **40,** 2198-205 (1969).

[23] H. E. Cook and J. E. Hilliard, Journal of Applied Physics **40,** 2191-8 (1969).

Figure captions

Figure 1. Cross sectional TEM image of a UHVCVD grown Si/SiGe superlattice, [Si 2.2 nm $Si_{0.85}Ge_{0.15}$ 6.1 nm]$_{20}$, typical of those employed in this study. The structure is grown directly onto a (100) Si substrate so that the SiGe layers are under compressive strain and the Si layers are largely unstrained. The overall film thickness is supercritical with respect to strain relaxation but the individual bilayers are subcritical; thus the misfit dislocation array will be restricted to the film/substrate interface. The structure is terminated with a Si layer to minimize surface roughening.

Figure 2. Concentration dependence of the exponential prefactor for SiGe self-diffusion. Data collected by Zangenberg et al[8] are shown along with the exponential curve fit used as an input for the interdiffusion simulations in this work.

Figure 3. Concentration dependence of the activation enthalpy for SiGe self-diffusion. Data collected by Zangenberg et al[8] are shown along with the curve fit used as an input for the interdiffusion simulations in this work. The shape of the curve was adjusted, within the experimental error, to obtain the best possible fit to our measured datasets. It is significant that the activation enthalpy remains nearly constant below for $X_{Ge} < 0.1$.

Figure 4. Initial condition and result of a 1.5 hour, 870 C interdiffusion simulation for the film shown in Fig. 1. Only the two lowermost bilayers are shown. The interfacial width and intralayer thickness variation present in the real film are represented in the

simulation as a sinusoidal concentration profile at the interfaces. To simulate diffusion into the substrate, the initial concentration profile used for the first bilayer includes a large field of zero concentration on the left hand side and a boundary condition of zero concentration at the right hand edge. Periodic boundary conditions are applied to all other bilayers so that any Ge diffusing out the left side of a bilayer is reintroduced on the right side and vice versa.

Figure 5. Simulated diffraction patterns for the Ge profiles that are partially illustrated in Fig. 4 (an as-deposited superlattice, and a 1.5 hour, 870 C interdiffusion simulation). For input into the diffraction simulation, the concentration profiles are discritized into thin slabs of constant concentration. The section of profile shown in Fig. 4, for example, was broken into approximately 300 slabs. The superlattice satellite peaks clearly decay as a result of interdiffusion. Since no roughening mechanisms are included in the simulation, the decaying thickness oscillation intensity is entirely due to introduction of a more gradual film/substrate interface.

Figure 6. Measured and simulated superlattice satellite intensity decay for the case illustrated in Figs. 1, 4, and 5. According to Eq. 1, the slopes of these curves are linearly proportional to interdiffusivity.

Figure 7. Diffraction simulations overlaid onto measured diffraction patterns. The sample structures used in these diffraction simulations were determined independently of the simulation and no effort was made to adjust the structural parameters to optimize the

fit shown here. (a) Result for as-grown structure illustrated in Fig. 1. (b) Structure illustrated in Fig. 1 after a 1.5 hour anneal at 870 C. The loss of fine detail in the measured diffraction pattern is probably due to out-of-plane roughening. (c) Results for as-grown case with structure [Si 5 nm $Si_{0.87}Ge_{0.13}$ 5.6 nm]$_{10}$.

Figure 8. Simulated superlattice satellite decay rates for the case of a concentration independent interdiffusivity (a) and the actual concentration dependent model employed in this work (b). In (a), Model output refers to a satellite decay rate calculated with Eq. 1 using the constant interdiffusivity employed in the simulation. In (b), Model output shows the decay calculated using Eq. 1 given the appropriate concentration dependent interdiffusivity values for the mean, maximum, and minimum Ge concentrations present in the structure as a function of annealing time. The FFT result in both plots shows the decay rate of the first order peak obtained by applying a finite Fourier transform to the concentration profiles produced by the interdiffusion simulation.

Figure 9. Simulation results showing concentration dependent interdiffusivity values as a function of annealing time for the mean, maximum, and minimum Ge concentrations present in the evolving structure. (a) A relatively low concentration film — [Si 5 nm $Si_{0.87}Ge_{0.13}$ 5.6 nm]$_{10}$. (b) A film with higher Ge concentration — [Si 2.2 nm $Si_{0.85}Ge_{0.15}$ 6.1 nm]$_{20}$.

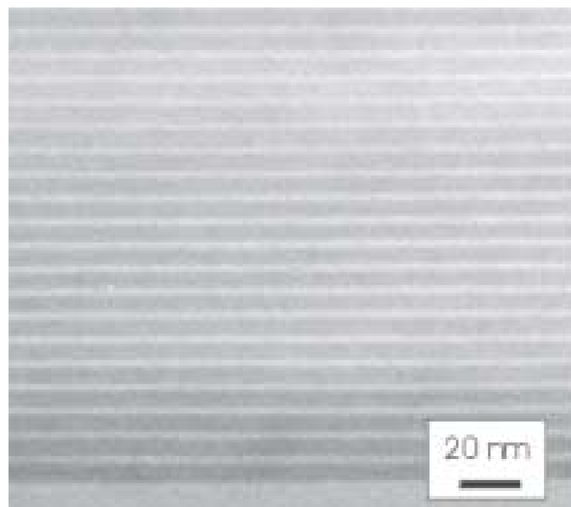
20 nm

Figure 2 D.B. Aubertine Journal of Applied Physics

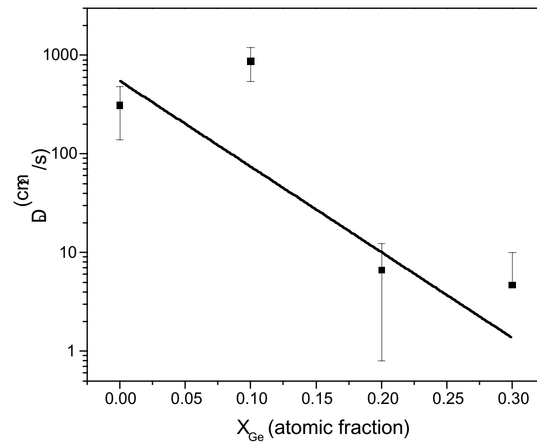

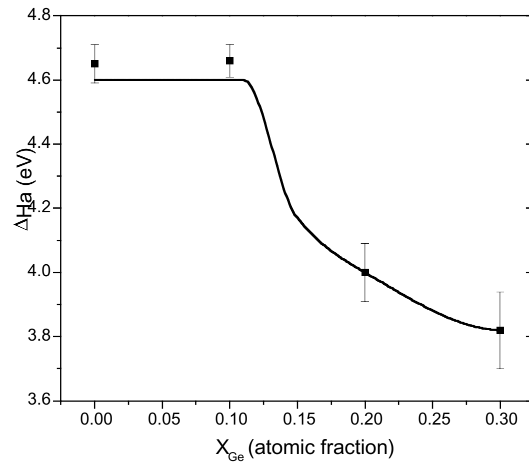

4.8
4.6
4.4
4.2
4.0
3.8
3.6
ΔHa (eV)
0.00
0.05
0.10
0.15
0.20
0.25
0.30
X_{Ge} (atomic fraction)

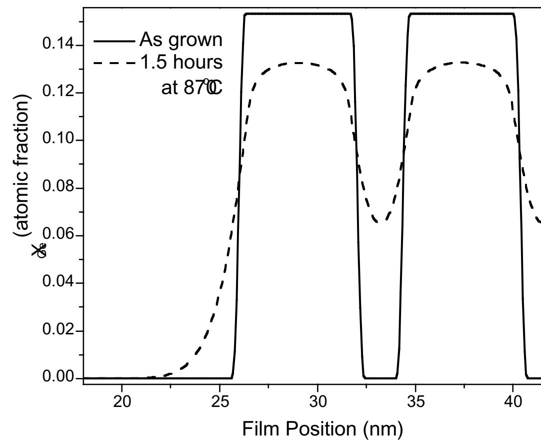
As grown
1.5 hours
at 870°C
x (atomic fraction)
Film Position (nm)
0.00
0.02
0.04
0.06
0.08
0.10
0.12
0.14
20
25
30
35
40

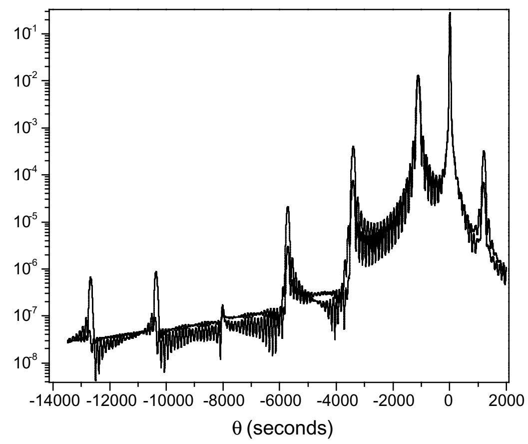

10^{-1}
10^{-2}
10^{-3}
10^{-4}
10^{-5}
10^{-6}
10^{-7}
10^{-8}
-14000 -12000 -10000 -8000 -6000 -4000 -2000 0 2000
θ (seconds)

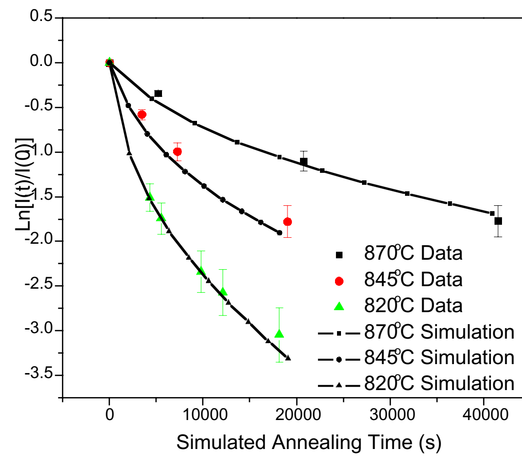

0.5
0.0
-0.5
-1.0
-1.5
-2.0
-2.5
-3.0
-3.5
Ln[I(t)/I(0)]
0
10000
20000
30000
40000
Simulated Annealing Time (s)
870°C Data
845°C Data
820°C Data
870°C Simulation
845°C Simulation
820°C Simulation

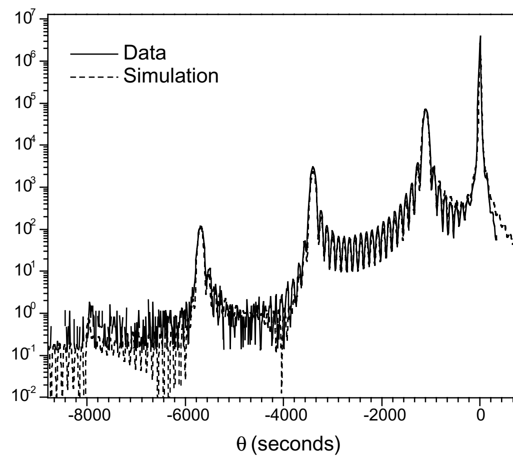

(a)

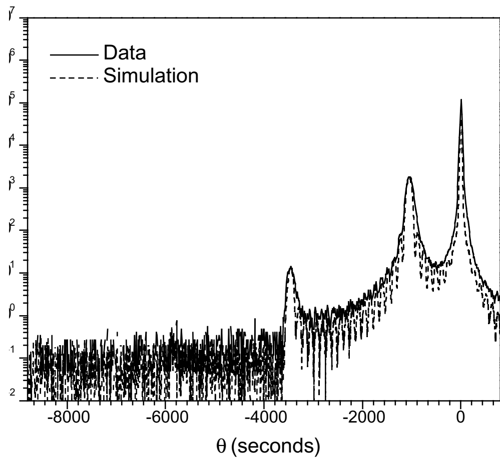

(b)

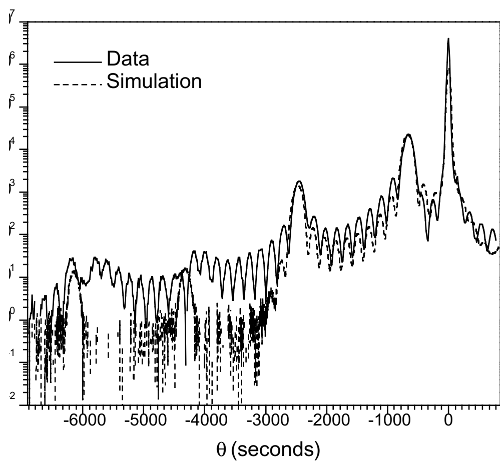

(c)

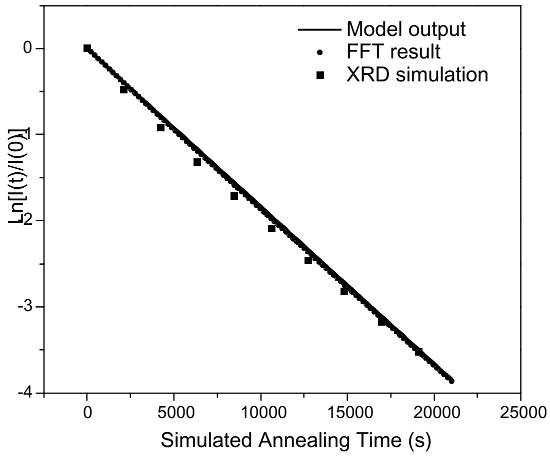

(a)

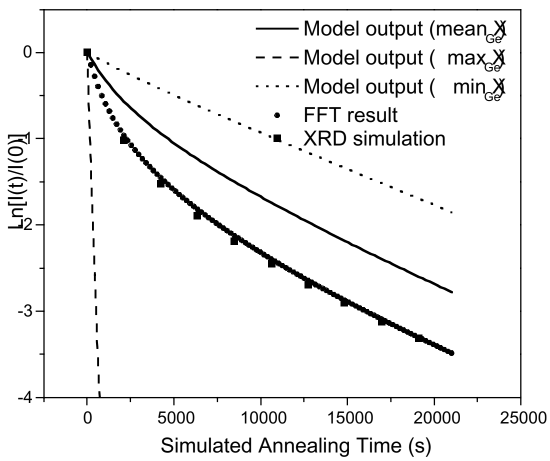

(b)

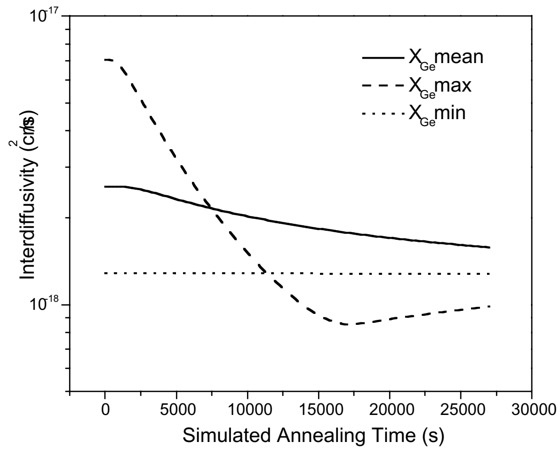

(a)

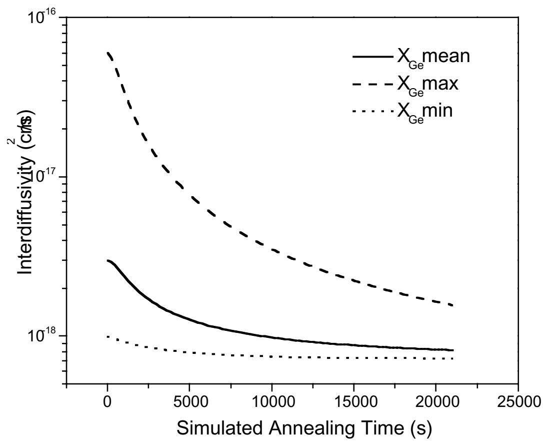

(b)